Film-forming Characteristics of Starches

Z. LIU AND J.H. HAN

ABSTRACT: Our objective was to understand the film-forming characteristics of amylose, amylopectin, and high-amylose (55%) starch solutions at ambient environment. By using an inverted phase-contrast microscope connected to an imaging system, we were able to record and analyze the microstructural evolution of starch throughout the process of film formation. The results of image analysis suggested that the coil-to-helix transition, followed by the helices aggregation, dominated the initial stage of starch film formation from solutions, although the time when these phenomena occurred depended on the amylose content. Fresh amylose films exhibited an assembly of giant dendrites with quarternary branches. In contrast, amylopectin films showed a structure of networked clusters. Interestingly, the high-amylose (55%) starch film showed a heterogeneous structure with both amylose-rich and amylopectin-rich phases, which are integrated seamlessly by the intermolecular interaction between amylose and amylopectin.

Keywords: starch, edible films, image processing, amylose, amylopectin

Introduction

Edible filmzs and coatings based on biopolymers have long been used for protecting foods and pharmaceuticals from moisture and oxygen invasion, as well as for carrying colorants and antimicrobial, flavoring, and leavening agents (Guilbert and others 1995). As a renewable biopolymer that has been massively produced worldwide (Liu 2002), starch is a relatively cost-effective choice compared with protein and wax as the foundation material for edible films and coatings (Wolff and others 1951; Mark and others 1966; Jokay and Mitan 1969). Furthermore, it is hihghly likely to customize starch-based edible films and coatings for desirable functionalities because of the availability of a wide variety of starches (Liu 2004), which may contain any amount of amylose or amylopectin through genetic engineering techniques (Davis and others 2003).

A high amylose content in starch is known to lead to strong and flexible films (Wolff and others 1951; Moore and Robinson 1968; Lourdin and others 1995; Palviainen and others 2001), probably due to the crystallization of amylose (van Soest and others 1996; Forssell and others 1999; Myllärinen and others 2002). Research on the crystallography of amylose has revealed A-, B- and V-type crystals (Whittam and others 1989; Welland and Donald 1991; Helbert and Chanzy 1994; Hulleman and others 1996). The A- and B-type amylose crystals are constructed by amylose double-stranded helices but with different packing modes (Wu and Sarko 1978a, 1978b). Water-cast amylose films often show B-type crystallization (Unbehend and Sarko 1974; Wu and Sarko 1978b; Myllärinen and others 2002). The V-type amylose crystal is based on left-handed single-stranded helices that are affiliated by some small molecules such as ethanol (Welland and Donald 1991), isopropanol (Buléon and others 1990), n-butanol (Helbert and Chanzy 1994), and glycerol (Hulleman and others 1996). Amylose-alcohol V-type microcrystals are often roughly square-, rectangular- or platelet-shaped; the crystals have an orthorhombic symmetry, and within the unit cell the amylose chains are organized in antiparallel pairs of parallel amylose helices with a number of precipitant molecules located between the helices (Buléon and others 1990; Helbert and Chanzy 1994; Hulleman and others 1996). Compared with amylose, amylopectin is relatively slow to crystallize by water evaporation (Goodfellow and Wilson 1990) because of its high molecular weight and hyperbranched structure. It may develop B-type crystals after long-period conditioning under high relative humidity (for example, 91%) (Myllärinen and others 2002). Regardless of the content of amylose in starch (Rindlav and others 1997), the degree of crystallinity for fresh starch films is very low (<10%) (Rindlav-Westling and others 1998; García and others 2000; Myllärinen and others 2002). Microscopically, starch films show either few interesting features (García and others 2000) or presumably a structure similar to that of starch gels, which resembles a network of rodlike strands (Unbehend and Sarko 1974; Leloup and others 1992; Rindlav-Westling and others 1998).

The objective of this work was to understand the microstructural development during drying of amylose, amylopectin, and high-amylose starch solutions, and the physical interaction between amylose and amylopectin, by analyzing time sequences of phase-contrast images. Understanding the film-forming characteristics is of practical importance to produce starch films or coatings with desirable microstructures that determine their performance.

Materials and Methods

Materials

Amylose (type III from potato, 2% butanol) was obtained from Sigma-Aldrich (St. Louis, Mo., U.S.A.), high-amylose (Hylon V, 55% amylose, hereafter called 50/50), and waxy (Amioca, >99% amylopectin) corn starches from National Starch & Chemical Co. (Bridgewater, N.J., U.S.A.).

Water-cast high-amylose starch film

Five grams of high-amylose starch (50/50) was dispersed in 95 g of deionized wtater and autoclaved at 127 °C for 20 min. After being autoclaved, the starch solution was cooled to 50 °C to 60 °C, and 9 g of the starch solution was transferred to a polystyrene petri dish (10-cm dia) placed on a well-leveled wood slab. The petri dish was dried for 24 h at ambient temperature to obtain a starch film on the petri dish surface. The film on the petri dish was directly used for microscopy experiment without peeling off the film from the petri dish.

MS 20040504 Submitted 7/28/04, Revised 9/13/04, Accepted 9/29/04. *Authors are with Dept. of Food Science, Univ. of Manitoba, Winnipeg, Manitoba, R3T 2N2, Canada. Direct inquiries to author Han (E-mail: hanjh@ms.umanitoba.ca).*

Preparation of starch solutions

Starch (0.02 g) was soaked in 2 mL of distilled water at 25 °C for 4 h in a capped test tube. After agitation, the capped tube was autoclaved at 127 °C for 20 min. After cooling to 100 °C in the autoclave, the capped tube was inserted into a heating block maintaining 95 °C preventing starch gelation. The hot solution in the tube was agitated and immediately filtered using a preheated syringe filter (average pore size, 0.45 μm). The filtrate was collected into another test tube in the same heating block, and the filtrate tube was then capped to prevent water evaporation. This sample solution was used immediately for photomicrography tests.

Visualization of starch film formation

A drop (about 0.2 mL) of the filtrates was placed onto a microscope slide at ambient environment (23 °C, 40% relative humidity) and observed using an inverted phase-contrast microscope (Nikon Diaphot TMD, Kanagawa, Japan) equipped with a TV camera (Panasonic WV-1550, Matsushita Electric Industrial Co., Ltd., Osaka, Japan). The transmitted light source in the microscope was a tungsten halogen bulb (12 V/50 W). An NCB10 (blue) color-correction filter (Nikon) was placed on the filter receptacle to reduce the spectral bandwidth of the source to the range of 430 to 530 nm. We used the DL (dark low) series of objectives (Ph1 10×, Ph2 20×, and Ph3 40×), which are designed to produce positive contrast in specimens having a significant difference in refractive index from the surrounding medium. A 2.5× relay lens was placed in the tube adapter connecting the TV camera to the microscope.

Phase-contrast microscopy is particularly powerful to produce high-contrast images of transparent or translucent specimens such as starch films. The inverted configuration, where the objective is placed underneath the specimens, and the condenser above the specimens, allows examining microstructural evolution of starch films without the risk of water vapor interfering with the objectives.

The whole process of film formation was monitored and recorded by a personal computer equipped with a video capture card. The image resolution was set at 640 × 480 pixels. The compression method used in video recording was Huffyuv codec (Ben Rudiak-Gould), which does not cause any loss in the video's original quality.

Image processing and analysis

The recorded videos in audio-video-interleave (AVI) format were converted to a time sequence of 8-bit grayscale images in bitmap (BMP) format, which were trimmed by 5 pixels per side to remove the unfocused areas.

An image analysis program (SigmaScan Pro 5.0, Statistical Solutions, Saugus, Mass., U.S.A.) was used to measure the dimensions of objects of interest (for example, dendrites, crystals) in the images, which were scaled by using a stage objective micrometer (0 to 1 mm/100).

The program was also used to obtain the grayscale images' intensity histograms, in which the number of pixels in the images with a particular intensity is collected as a function of the pixels' intensity. Denoted by a grayscale level, the pixel intensity describes how dark or bright a pixel in an image is. For 8-bit images, the pixel intensity is assigned a value between 0 and 255. The higher the number, the brighter the pixel represents. A macro (in Visual Basic for Applications) was coded to calculate the average pixel intensity (so-called image intensity) and its standard deviation (intensity stdev) from the intensity histogram data. While a higher value of image intensity corresponds to an overall brighter image, a higher value of standard deviation indicates a broader distribution of the pixel intensities in the image.

The intensity of each pixel in a phase-contrast image is primarily related to the optical path length, which is a product of the refractive index and specific thickness of the component that the pixel represents in a specimen. Therefore, the image intensity can be used as a gauge for approximating relationships between various components or structures in the specimen. When the refractive indices of the components (for example, amylose or amylopectin) are different from those of the surrounding medium (for example, water here), the components show up against the background in the phase-contrast image. Because the refractive indices of the components are related to their microstructures and/or densities, any changes in the microstructures and/or densities would (for example, coil-like "free" amylose molecules converting to ordered double helices, or aggregation of helices) consequently be reflected in the image intensity of the phase-contrast image, providing that the intensity of light source remains constant. Normally, higher refractive index of the components leads to lower image intensity for positive contrast images as in our case.

Drying of a drop of distilled water was recorded, image processed, and analyzed as mentioned previously. In 460 s, the image intensity remains nearly constant at 60 with a standard deviation of 16 (Figure 1), suggesting the negligible effect of water evaporation on the image intensity and standard deviation. Only when the droplet is partially dried (after 460 s of drying) and a contrast shows against the microscope slide in the view field, peaks in both average intensity and standard deviation are observed (Figure 1).

Results and Discussion

Because starch films are normally prepared by casting gelatinized starch dispersions where many swollen starch granules are often present (Zobel 1984), it is not surprising that starch films are often microscopically featureless (García and others 2000), due to the dominating compaction of those granular remnants that overshadow the possible microstructural development. The image of a water-cast high-amylose starch film made from 5% 50/50 (Hylon V) resembles a messy mixture of granular remnants (Figure 2), probably linked by amylose exuded during starch gelatinization (Zobel 1984). As with latex dispersions (DuChesne and others 1999), the 5% 50/50 dispersions formed films through aggregation and compaction of swollen starch granules, probably driven by water evaporation. The same pattern was observed from the 5% amylopectin solutions (data not shown).

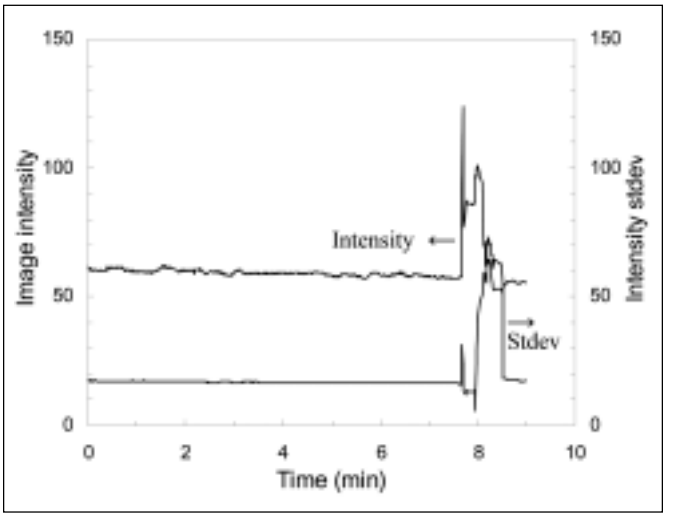

Figure 1—Development of image intensity and intensity standard deviation (stdev) with time for distilled water

Amylose films

It took about 35 min for a drop of amylose aqueous solutions to dry up and form a film. Multiple transitions were observed on the plot of image intensity (brightness) and intensity stdev as the drying proceeds (Figure 3). The increasing image intensity (brightness) in the 1st 5 to 11 min was presumably attributed to the known coil-to-helix transition (Wilson and others 1987; Goodfellow and Wilson 1990), by which the fully solubilized amylose molecules associate with each other to form double-stranded helices upon cooling from 95 °C to 23 °C. The corresponding peak on the standard deviation curve indicates that the helix formation is a heterogeneous or random transition process. Although the amylose solution concentrates with water evaporation, the image intensity hardly changed, due to the stability of amylose helices in the very dilute solution. The helices has little chance to precipitate (Gidley and Bulpin 1989), because the degree of polymerization of our potato amylose is in the range of 4920 – 5500 (Takeda and others 1984; Sievert and Wuersch 1993). However, when the critical gelation concentration is reached at about 28 min (Figure 3), the solution starts to gelate due to the aggregation of helices, which forms amylose microcrystals (Gidley 1989). High refractive index of the amylose microcrystals relative to that of the surrounding medium (that is, water) leads to the decreasing image intensity from 28 min (Figure 3). The gelating process was finished in about 4 min from minute 28 to minute 32 (Figure 3). Shortly afterward, the image intensity showed a peak transition (minute 36 to 38) (Figure 3), which was attributed to the formation of amylose films through rearrangement of those microcrystals or aggregation with patterns (Wu and Sarko 1978a, 1978b).

Interestingly, the amylose films showed a pattern of dendrites. As with the crystallization of ice (Gonda and Nakahara 1996) and metallic alloys (Glicksman 1990; Trivedi 1990), the primary dendrites of amylose grow in water phase of amylose solution while 90 degree side-branching (Figure 4). It is plausible that the dendritic growth is driven by supersaturation of amylose due to water evaporation according to De Goede and Van Rosmalen (1990). Figure 5 shows the longitudinal growth rates of 2 dendrites (d1 and d2) selected on Figure 4. Apparently, both dendrites initially grew at the same rate of about 27 μm/s. After growing steadily for about 5 s, dendrite d2 accelerated after the dendrite closely approaches the

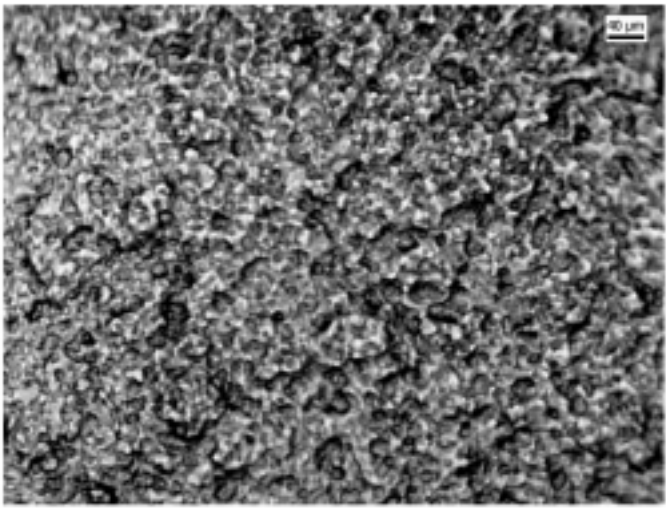

Figure 2—Photomicrograph of Hylon V film (5% dispersion casting)

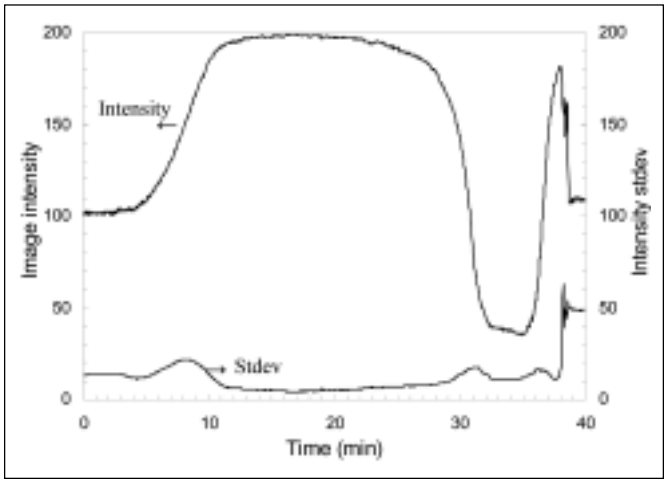

Figure 3—Development of image intensity and intensity standard deviation (stdev) with time for 1% aqueous amylose solutions

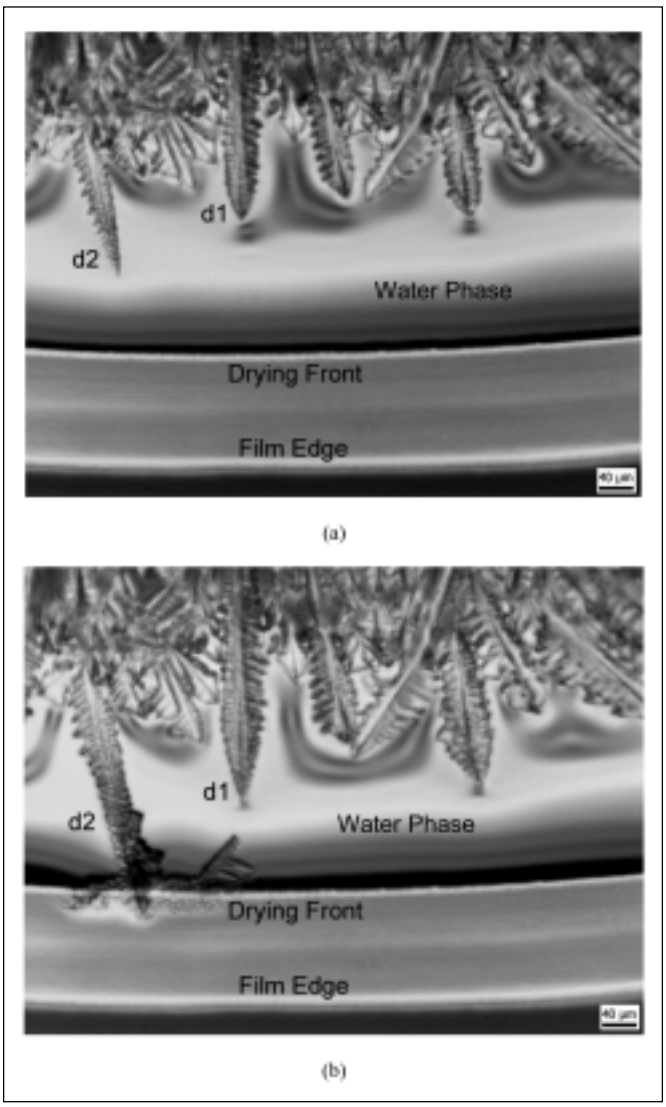

Figure 4—Growing amylose dendrites at 2305 s (a) and those at 4 s later (b)

water boundary (drying front), whereas dendrite d1 slowed down. The higher growth rate of d2 is presumably caused by the higher local supersaturation of amylose in its vicinity that has been demonstrated by De Goede and Van Rosmalen (1990).

Unlike n-butanol precipitated amylose, which look like either large, well-formed, 6-pedaled rosettes (50 to 80 μm in diameter) or clumps of hairlike needles (Schoch 1942), the amylose film so prepared featured a layer of packed "giant" dendrites (Figure 6). The dendrites grow continuously with 90-degree branching, which possesses a perfect pattern of fractals. Exhibiting a hierarchy of 4 levels (Figure 6a), these quarternary dendrites were characterized by unique crossed primary branches, the diameter of which was 1 to 2 μm. Like other crystalline polymers such as polypropylene, which shows boundaries between spherulites (Feng and others 2000), amylose dendrites stop growing where any 2 dendrites meet, leaving behind distinct boundaries (Figure 6b).

Amylopectin films

A number of transitions in image intensity and intensity stdev were also observed during the film formation of amylopectin solutions (Figure 7). The 1st one is a sharp increase in the image intensity occurring by 8 s (Figure 7 inset), due to the intramolecular coil-to-helix transition of amylopectin branches, which is known as a much faster process than the intermolecular coil-to-helix transition of amylose (Goodfellow and Wilson 1990). Immediately afterward, the image intensity dropped from 112 to 82 in 7 min, whereas the intensity stdev remained at 45 (Figure 7). This intensity transition presumably reflects the aggregation of intermolecular helices, by which amylopectin molecules are gelated together. Afterward, the image intensity showed little change with time, which may indicate the slow aggregation and completion of aggregation of intramolecular double-stranded helices and form gel particles according to the result of Goodfellow and Wilson (1990).

In addition to transparency, the amylopectin film did show an interesting microstructure pattern, which is an assembly of interlinked clusters (Figure 8a). Zooming in the structure unraveled a biphasic structure, where clusters of particles were embedded in an amorphous background (Figure 8b). Diameter of the particles was 1 to 2 μm, the same as that of the strands constructing the primary branches in amylose dendrites (Figure 6). It is suggested that the network of clusters resulted from association of both intramo-

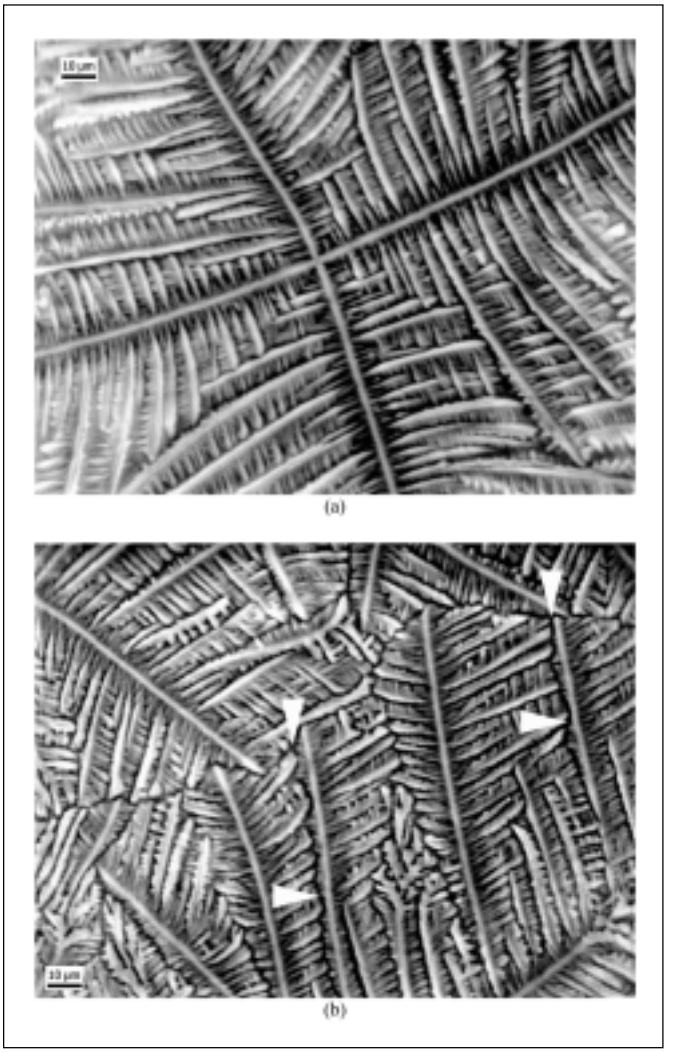

Figure 6—Photomicrographs of amylose films showing a dendrite center (a) and boundaries (white arrow heads) between dendrites (b)

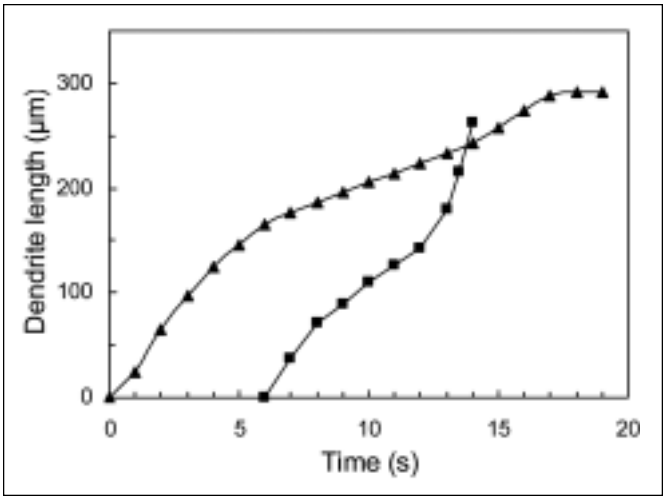

Figure 5—Growth of amylose dendrites d1 (▲, see Figure 4a) and d2 (■, see Figure 4b). The origin of time axis corresponds to the 2293rd s on the time axis of Figure 4.

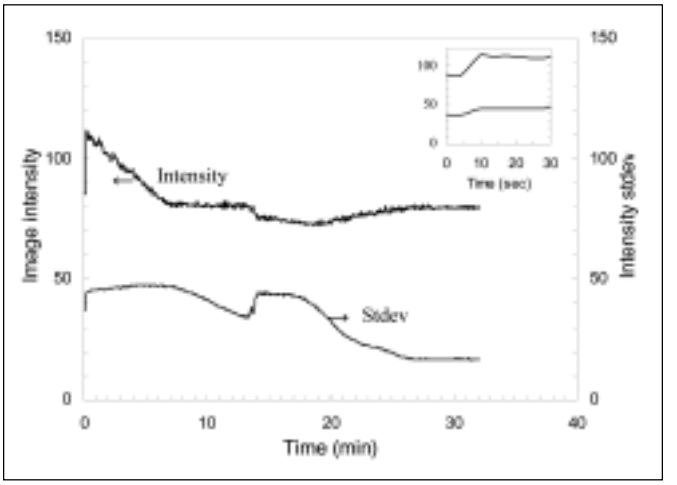

Figure 7—Development of image intensity and intensity standard deviation (stdev) with time for 1% aqueous amylopectin solutions. The inset shows the development in the 1st 30 s.

lecular and intermolecular double helices, and the amorphous background is made of the chain segments that constituent the amorphous lamellae in amylopectin, which also has been suggested by Daniels and Donald (2004).

Amylose/amylopectin (50/50) films

Three major transitions were observed for the film formation of 50/50 (Hylon V) solutions (Figure 9). The 1st transition occurring in the 1st 5 min was presumably attributed to the coil-to-helix transition of amylopectin intramolecular branches, whereas the 3rd transition occurring between 12 and 18 min to the coil-to-helix transition of amylose molecules because the former normally proceeds faster than the latter (Goodfellow and Wilson 1990). The 2nd transition between 5 and 12 min (Figure 9) is supposedly a result of double-helix formation of amylose molecules and amylopectin side-branches. The premise is that amylose can interact with amylopectin in gels or aqueous solutions. It has actually been found that the 2 components can co-crystallize (Rindlav-Westling and others 2002) and that the presence of amylopectin tends to stabilize the solutions of amylose wrapped single-wall nanotubes (Star and others 2002). On this basis, we suggested that both molecular and supramolecular interaction could occur. At molecular level, amylose molecules associate

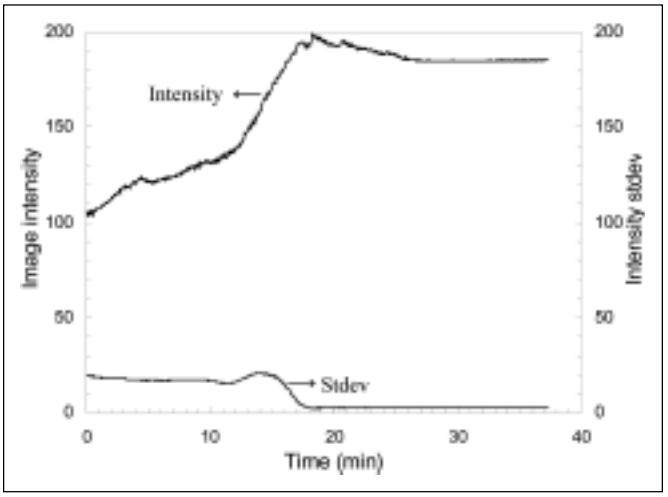

Figure 9—Development of image intensity and intensity standard deviation (stdev) with time for 1% aqueous amylose/amylopectin (50/50) solutions

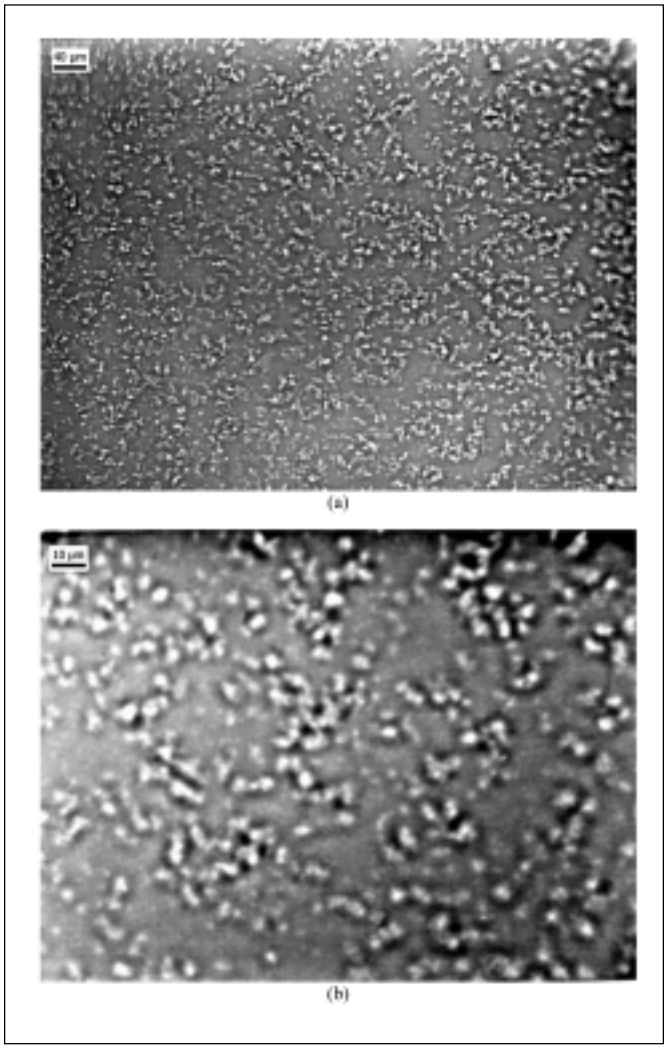

Figure 8—Photomicrographs of amylopectin film at low magnification (a) and high magnification (b)

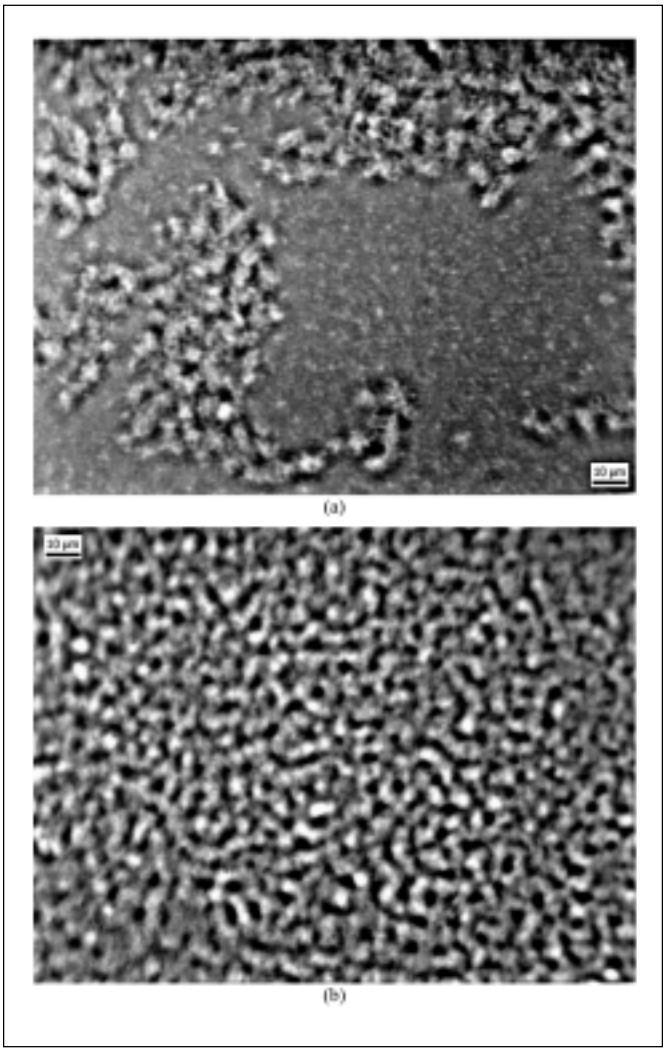

Figure 10—Microstructures of amylose/amylopectin (50/50) film: (a) phase separation; (b) network of high-amylopectin region

with amylopectin branches to form double helices, as probably indicated by the 2nd transition (Figure 9). At supramolecular level, the double helices of amylose bundle with those of amylopectin. The amylose/amylopectin interaction at both molecular and supramolecular levels leads to the formation of crosslinked giant molecules, which would present a great stereochemical hindrance for the double helices of amylose, amylopectin, or both to aggregate. The slight decrease in the image intensity between 18 and 26 min possibly reflects the limited aggregation of the double helices in the solution.

The water-cast 50/50 films exhibit a biphasic structure (Figure 10), which is consistent with the findings of Rindlav-Westling and others (2002). In general, the structure resembles a network of clusters embedded in an amorphous background (Figure 10a). As in the amylopectin films (Figure 8), the amorphous phase in the 50/50 films was composed of amorphous amylopectin chain segments. However, the network phase for the 50/50 films show better connectivity (Figure 10b) than the amylopectin films (Figure 8b), even though the diameter of the particles is still in the range of 1 to 2 μm. We believe that the network phase was composed of bundles of double helices of amylose, amylopectin, or both. It is not surprising that no pattern of dendritic growth was observed for the 50/50 films, which contains 55% amylose, because the molecular and supramolecular interaction between amylose and amylopectin leads to the formation of giant molecules. Moreover, no visible boundaries exist between the network and amorphous phases because the 2 phases were molecularly or supramolecularly integrated via the formation or aggregation of double helices.

Conclusions

The mechanisms of starch film formation depend on the solid concentration and amylose content. Generally, aggregation and packing of swollen granules dominated the film formation of starch dispersions with a relatively high solid concentration. However, both coil-to-helix transition and aggregation of double helices are operative during the film formation from dilute starch solutions. Nonetheless, the amylose content showed significant effects on the moment when and the extent to which the double helices form and aggregate. Among the 3 specimens examined, amylose solution exhibited the most significant helical formation and aggregation. In summary, the film formation of dilute starch solutions follows the order of helical formation, aggregation or gelating, and reorganization of aggregates; the former was primarily driven by cooling and the latter 2 by dehydration.

Amylose films exhibited a pattern of 4-fold dendrites, whereas amylopectin films showed a biphasic structure, in which a network of clusters was embedded in an amorphous background. Amylose/amylopectin (50/50) films showed a biphasic structure similar to that of amylopectin. The 2 phases are integrated by molecular and supramolecular interaction between amylose and amylopectin through helical formation and bundling.

Acknowledgments

The authors thank Natural Sciences and Engineering Council (NSERC) of Canada and Western Grain Research Foundation (WGRF) for the research grant.

References

Buléon A, Delage MM, Brisson J, Chanzy H. 1990. Single crystals of V amylose complexed with isopropanol and acetone. Int J Biol Macromol 12:25–33.
Daniels DR, Donald AM. 2004. Soft material characterization of the lamellar properties of starch: smectic side-chain liquid-crystalline polymeric approach. Macromolecules 37:1312–8.
Davis JP, Supatcharee N, Khandelwar RL, Chilbbar RN. 2003. Synthesis of novel starches in planta: opportunities and challenges. Starch/Stärke 55:107–20.
De Goede R, Van Rosmalen GM. 1990. Crystal growth phenomena of paraxylene crystals. J Crystal Growth 104:399–410.
DuChesne A, Bojkova A, Rottstegge J, Glasser G, Neher D, Krieger S. 1999. Film formation of heterogeneous latex systems - a comparative study by mechanical testing, electron microscopy, interferometry and solid state NMR. Phys Chem Chem Phys 1:3871–8.
Feng Y, Liu Z, Yi XS. 2000. Co-occurrence of photochemical and thermal effects during laser polymer ablation via a 248-nm excimer laser. Appl Surf Sci 156:177–82.
Forssell P, Hulleman S, Myllärinen P, Moates G, Parker R. 1999. Ageing of rubbery thermoplastic barley and oat starches. Carbohydr Polym 39:43–51.
García MA, Martino MN, Zaritzky NZ. 2000. Microstructural characterization of plasticized starch-based films. Starch/Stärke 52:118–24.
Gidley MJ. 1989. Molecular mechanisms underlying amylose aggregation and gelation. Macromolecules 22:351–8.
Gidley MJ, Bulpin PV. 1989. Aggregation of amylose in aqueous systems: the effect of chain length on phase behavior and aggregation kinetics. Macromolecules 22:341–6.
Glicksman ME. 1990. Fundamentals of dendritic growth. In: Trivedi R, Sekhar JA, Mazumdar J, editors. Principles of solidification and materials processing. Aedermannsdorf, Switzerland: Trans Tech Publications. p 12–32.
Gonda T, Nakahara H. 1996. Formation mechanism of side branches of dendritic ice crystals grown from vapor. J Crystal Growth 160:162–6.
Goodfellow BJ, Wilson RH. 1990. A Fourier transform infrared study of the gelation of amylose and amylopectin. Biopolymers 30:1183–9.
Guilbert S, Gontard N, Cuq B. 1995. Technology and applications of edible protective films. Packag Technol Sci 8:339–46.
Helbert W, Chanzy H. 1994. Single crystals of V amylose complexed with n-butanol or n-pentanol: structural features and properties. Int J Biol Macromol 16:207–13.
Hulleman SH, Helbert W, Chanzy H. 1996. Single crystals of V amylose complexed with glycerol. Int J Biol Macromol 18:115–22.
Jokay L, Mitan FJ. 1969. Process of coating food. American Maize-product Co. 1969 Feb 18. U.S. Patent 3,427,951.
Leloup VM, Colonna P, Ring SG, Roberts K, Wells B. 1992. Microstructure of amylose gels. Carbohydr Polym 18:189–97.
Liu Z. 2002. Starch: from granules to biomaterials. In: Pandalai SG, editor. Recent research developments in applied polymer science. Vol. 1, Part 1. Trivandrum, India: Research Signpost. p 189–219.
Liu Z. 2005. Edible films and coatings from starches. In: Han JH, editor. Innovations in food packaging. Amsterdam: Elsevier. Forthcoming.
Lourdin D, Della Valle G, Colonna P. 1995. Influence of amylose content on starch films and foams. Carbohydr Polym 27:261–70.
Mark AM, Roth WB, Mehltretter CL, Rist CE. 1966. Oxygen permeability of amylomaize starch films. Food Technol 20:75–7.
Moore CO, Robinson JW. 1968. Method for coating fruits. AE Staley Manufacturing Co. 1968 Feb 13. U.S. Patent 3,368,909.
Myllärinen P, Buléon A, Lahtinen R, Forssell P. 2002. The crystallinity of amylose and amylopectin films. Carbohydr Polym 48:41–8.
Palviainen P, Heinämäki J, Myllärinen P, Lahtinen R, Yliruusi J, Forssell P. 2001. Corn starches as film formers in aqueous-based film coating. Pharm Develop Technol 6:353–61.
Rindlav A, Hulleman SHD, Gatenholm P. 1997. Formation of starch films with varying crystallinity. Carbohydr Polym 34:25–30.
Rindlav-Westling A, Stading M, Gatenholm P. 2002. Crystallinity and morphology in films of starch, amylose and amylopectin blends. Biomacromolecules 3:84–91.
Rindlav-Westling A, Stading M, Hermansson AM, Gatenholm P. 1998. Structure, mechanical and barrier properties of amylose and amylopectin films. Carbohydr Polym 36:217–24.
Schoch TJ. 1942. Fractionation of starch by selective precipitation with butanol. J Am Chem Soc 64:2957–61.
Sievert D, Wuersch P. 1993. Thermal behavior of potato amylose and enzyme-resistant starch from maize. Cereal Chem 70:333–8.
Star A, Steuerman DW, Heath JR, Stoddart JF. 2002. Starched carbon nanotubes. Angew Chem Int Ed 41:2508–12.
Takeda Y, Shirasaka K, Hizukuri S. 1984. Examination of the purity and structure of amylose by gel-permeation chromatography. Carbohydr Res 132:83–92.
Trivedi R. 1990. Directional solidification of alloys. In: Trivedi R, Sekhar JA, Mazumdar J, editors. Principles of solidification and materials processing. Aedermannsdorf, Switzerland: Trans Tech Publications. p 32–65.
Unbehend JE, Sarko A. 1974. Light scattering and x-ray characterization of amylose films. J Polym Sci Polym Phys Ed 12:545–54.
van Soest JJG, Hulleman SHD, de Wit D, Vliegenthart JFG. 1996. Changes in the mechanical properties of thermoplastic potato starch in relation with changes in B-type crystallinity. Carbohydr Polym 29:225–32.
Welland EL, Donald AM. 1991. Single crystals of V amylose. Int J Biol Macromol 13:69–72.
Whittam MA, Orford PD, Ring SG, Clark SA, Parker ML, Cairns P, Miles MJ. 1989. Aqueous dissolution of crystalline and amorphous amylose-alcohol complexes. Int J Biol Macromol 11:339–44.
Wilson RH, Kalichevsky MT, Ring SG, Belton PS. 1987. A Fourier-transform infrared study of the gelation and retrogradation of waxy-maize starch. Carbohydr Res 166:162–5.
Wolff IA, Davis HA, Cluskey JE, Gundrum LJ, Rist CE. 1951. Preparation of films from amylose. Ind Eng Chem 43:915–9.
Wu HCH, Sarko A. 1978a. The double-helical molecular structure of crystalline α-amylose. Carbohydr Res 61:27–40.
Wu HCH, Sarko A. 1978b. The double-helical molecular structure of crystalline B-amylose. Carbohydr Res 61:7–25.
Zobel HF. 1984. Gelatinization of starch and mechanical properties of starch pastes. In: Whistler RL, BeMiller JN, Paschall EF, editors. Starch: chemistry and technology. New York: Academic Press. p 285–309.